High-entropy intermetallics serve an ultrastable single-atom Pt for propane dehydrogenation

Yuki Nakaya,[a] Eigo Hayashida,[a] Hiroyuki Asakura,[b] Ken-ichi Shimizu,[a,b] Shinya Furukawa*[a,b,c]

[a] Y. Nakaya, E. Hayashida, Prof. Dr. K. Shimizu, Prof. Dr. S. Furukawa,
Institute for Catalysis, Hokkaido University, N-21, W-10, Sapporo, Kita-ku, 001-0021 (Japan)
E-mail: furukawa@cat.hokudai.ac.jp
[b] Dr. H. Asakura, Prof. Dr. K.Shimizu, Prof. Dr. S. Furukawa,
Elements Strategy Initiative for Catalysts and Batteries, Kyoto University, Katsura, Nishikyo-ku, Kyoto, 615-8520 (Japan)
[c] Prof. Dr. S. Furukawa,
Japan Science and Technology Agency, Department of Research Promotion, Chiyoda, Tokyo 102-0076 (Japan)

Abstract: Propane dehydrogenation (PDH) has been a promising propylene production process that can compensate for the increasing global demand for propylene. However, Pt-based catalysts with high stability at ≥600°C have barely been reported because the catalysts typically result in short catalyst life owing to side reactions and coke formation. Herein, we report a new class of heterogeneous catalysts using high-entropy intermetallics (HEIs). Pt–Pt ensembles, which cause side reactions, are entirely diluted by the component inert metals in PtGe-type HEI; thereby, unfavorable side reactions are drastically inhibited. The resultant HEI: (PtCoCu)(GeGeSn)/Ca–SiO_2 exhibited an outstandingly high catalytic stability, even at 600°C ($k_d^{-1} = \tau = 4146$ h = 173 d), and almost no deactivation of the catalyst was observed two months for the first time.

Propylene is one of the most important basic raw materials in the petrochemical industry, which has been increasingly scarce due to the shale gas revolution (*1–6*). On-purpose propylene production *via* selective propane dehydrogenation (PDH) into propylene has been regarded as the most promising propylene production technology compared with other methanol-to-olefins and Fischer-Tropsch-to-olefins because of high propylene selectivity to meet the increasing global demand for propylene. However, due to its endothermicity, PDH requires high operation temperatures (>600°C) to obtain sufficient propylene yield, in which severe catalyst deactivation by coking and/or sintering inevitably occurs in short periods. In this context, developing an innovative PDH catalyst that exhibits high propylene selectivity and catalyst stability even at ≥600°C is incredibly beneficial for the chemical industry. Although numerous efforts have been made to overcome this obstacle, no outstandingly stable catalyst has yet been found to function for several months without deactivation.

PDH is a structure-insensitive reaction, whereas the undesired side reactions leading to deactivation, such as hydrogenolysis, clacking, and coking, are structure-sensitive (*1–6*). Active metal-metal ensembles such as Pt–Pt sites are known to induce these side reactions. Therefore, the dilution or isolation of Pt–Pt ensembles by an inert metal has been commonly employed as a standard catalyst design concept for selective and stable PDH (*1–7*). Single-atom-alloys (SAAs) (*8*), where Pt atoms are isolated by excess counterpart metal such as Cu, are the representative material/approach for this purpose; the undesired propylene decomposition is successfully inhibited over Pt@Cu SAA. However, SAAs typically undergo significant aggregation at ≥600°C due to the insufficient thermal stability, resulting in an irreversible deactivation of the catalyst. Therefore, a novel material that serves isolated Pt with high thermal stability is required to develop an ultrastable catalytic system for PDH.

The thermal stability of an alloy can be improved by increasing the number of constituent elements due to the significant contribution of mixing entropy, as observed for high-entropy alloys (HEAs: solid-solution alloys comprising five or more elements with near equimolar ratio) (*9–11*). Because of the unique characteristics and remarkable performances, the catalytic application of HEAs has received significant attention and amid the "gold rush" in recent years (*12*). However, for a random alloy structure, a large excess (>20 equiv.) of counterpart metals is needed for the complete isolation of Pt (*8*)(*13*). Therefore, there remain some Pt–Pt sites in a common (quinary to octonary) HEA. Thus, a multimetallic alloy with a particular ordered structure should be constructed to overcome this challenge. A possible candidate for such an ideal active site structure is high-entropy intermetallics (HEIs). Unlike HEAs, the constituent metals of an HEI are distributed separately to two (or more) crystallographically distinct sites, depending on the parent intermetallic structure (*14–18*). Scheme 1 illustrates the specific catalyst design concept employed in this regard. We focused on PtGe as the parent binary intermetallics (FeAs-type structure, space group: *Pnma*) due to its unique ordered surface structure and significantly negative formation enthalpy ($\Delta H_f = -90.8$ kJmol^{-1}) (*19*). The former provides one-dimensionally aligned Pt columns separated by Ge columns, where the surface Pt–Pt coordination number is only two (Scheme 1A). Besides, the latter can be the driving force to retain the ordered structure upon multi-metallization. Here, the Pt and Ge sites in PtGe are partially substituted by much less-active transition (Co and Cu) and inert typical (Ga and Sn) metals, respectively to form a senary HEI, i.e., ($Pt_xCo_{0.5-x/2}Cu_{0.5-x/2}$) ($Ge_{0.33}Ga_{0.33}Sn_{0.33}$) (hereafter, denoted as

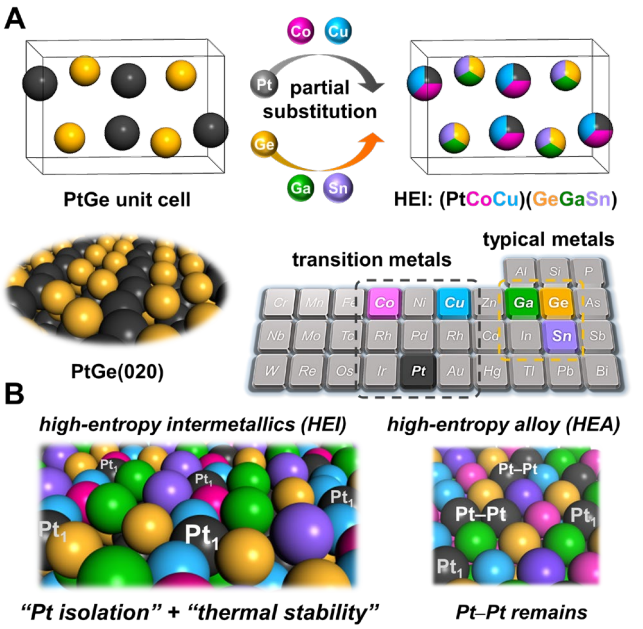

Scheme 1. The catalyst design concept for thermally stable isolated Pt site using HEI. (**A**) Pt and Ge sites in intermetallic PtGe are partially substituted by Co(Cu) and Ga(Sn), respectively, resulting in the formation of PtGe-type HEI (PtCoCu)(GeGaSn). (**B**) Illustrations of the (020) surface of (PtCoCu) (GeGaSn) HEI (left) and (111) surface of Pt-based senary HEA (right).

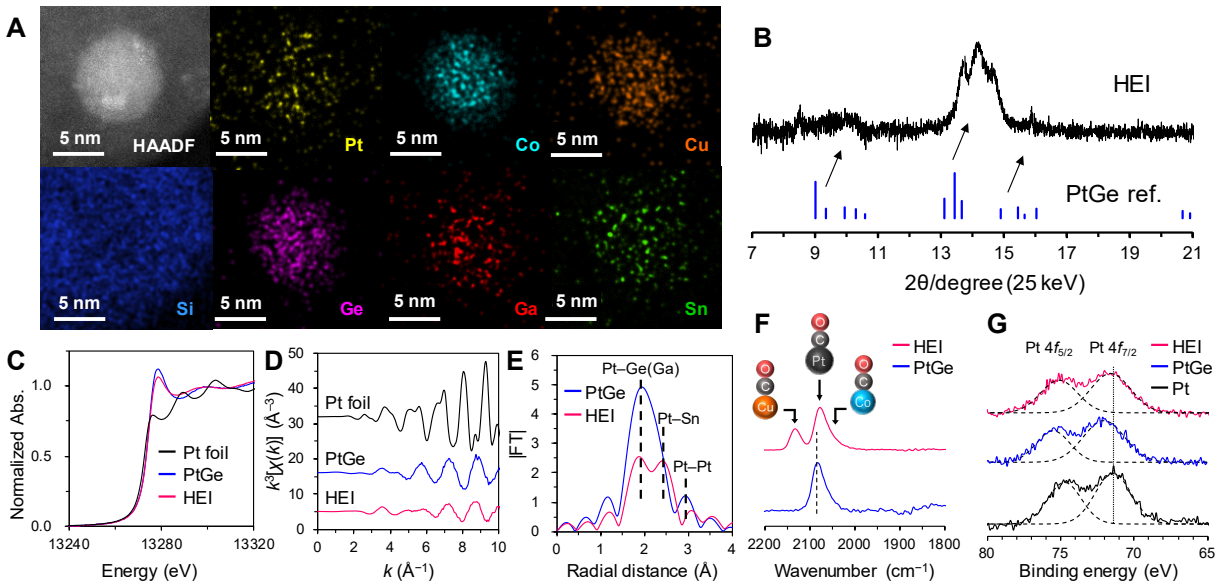

Fig. 1. Characterization of the HEI(0.25) catalyst. (**A**) HAADF-STEM image and the corresponding elemental maps for a single nanoparticle. (**B**) Synchrotron XRD pattern. Pt L_{II}-edge (**C**) XANES, (**D**) k^3-weighted EXAFS oscillations, and (**E**) Fourier-transformed EXAFS of Pt foil, PtGe/Ca–SiO_2, and HEI(0.25). (**F**) FT-IR spectra of CO adsorbed on PtGe/Ca–SiO_2 and HEI(0.25) at −100°C. (**G**) XPS of Pt/Ca–SiO_2, PtGe/Ca–SiO_2, and HEI(0.25).

HEI(x)). This site-specific multi-metallization allows the isolation of Pt by Co and Cu and further enhancement in thermal stability. Moreover, the degree of Pt isolation can be tuned by changing the Pt fraction x. This study reports a novel catalyst material and design concept based on HEIs, providing thermally stable isolated Pt and working as an outstandingly stable catalyst for high-temperature PDH.

The HEI catalysts were prepared by a pore-filling impregnation method as supported nanoparticles using Ca-modified amorphous silica (Ca–SiO_2, Supplementary materials, tables S1-S2, and fig. S1). The high-angle annular dark field scanning transmission electron microscopy (HAADF-STEM) analysis showed that nanoparticle size ranged 1–5 nm (average: 2.2 nm, fig. S2). Fig. 1A shows the elemental maps of a single nanoparticle obtained using the energy-dispersive X-ray analysis, confirming that the nanoparticle comprised Pt, Co, Cu, Ge, Ga, and Sn. Quantitative analysis for some small nanoparticles revealed that the atomic ratios of (Pt+Co+Cu)/(Ge+Ga+Sn) were close to unity (fig. S3). Fig. 1B shows the synchrotron X-ray diffraction (XRD) pattern of the HEI(0.25) catalyst, showing a PtGe-type diffraction pattern, unlike fcc- or hcp-type HEAs (*12*). The diffraction angles for the HEI were higher than those of the parent PtGe, attributed to lattice shrinkage by substituting Pt with the smaller size elements, Co and Cu (Supplementary Text 1 and tables S3-S4). We also performed X-ray absorption fine structure (XAFS) analysis to obtain further structural information (figs. S4, S5, and table S5 for the X-ray absorption near edge structure (XANES) spectra, extended XAFS (EXAFS) oscillations, and curve fittings, respectively). Fig. 1C shows the Pt L_{II}-edge XANES spectra of Pt foil, PtGe/Ca–SiO_2, and HEI(0.25) (figs. S6-S7 and table S6 for the structural analysis for PtGe/Ca–SiO_2). HEI(0.25) has a XANES characteristic that was similar to PtGe but different from Pt foil. In the raw EXAFS oscillations, a similar tendency was seen (Fig. 1D). Notably, the EXAFS oscillation of HEI(0.25) did not match with PtGa and PtSn (fig. S6 and table S6), supporting that the HEI retains the PtGe-type crystal structure. Further structural information is presented in the Fourier-transformed EXAFS spectra. Unlike PtGe, HEI(0.25) showed two peaks at 2.0 Å and 2.5 Å (Fig. 1E), which could be assigned to Pt–Ge(Ga) and Pt–Sn scatterings, respectively (table S5), demonstrating that Sn is doped into the Ge site. Besides, the Pt–Pt scattering at 3.0 Å, observed for PtGe, disappeared upon the multi-metallization. This suggests that Pt atoms were sufficiently isolated by substitution with Cu and Cu. We also performed comparable analyses for absorption edges other than Pt L_{II}, where curve fitting allowed use to assign all of the associated transition–typical metal scatterings (Co–Ge(Ga), Cu–Sn, Ga–Co(Cu), and Sn–Pt, for example, fig. S5 and table S5). (For a more detailed discussion of the EXAFS analysis, see Supplementary Text 2). These results comprehensively support the formation of the (PtCoCu)(GeGaSn) structure.

Next, the surfaces of PtGe and HEI were analyzed by Fourier-transform infrared (FT-IR) spectroscopy with CO adsorption at −100°C (Fig. 1F). For PtGe, a peak assigned to linearly adsorbed CO on Pt atoms appeared at 2080 cm^{-1} (*20*, *21*). For HEI(0.25), two kinds of linear CO were observed at 2070 cm^{-1} and 2150 cm^{-1}, assignable to those on Pt (*20*, *21*) and Cu (*22*), respectively. The broad shoulder peak at 2024 cm^{-1} may be attributed to linear CO on Co (*23*). For both catalysts, no absorption was observed below 2000 cm^{-1}, indicating the absence of three-fold Pt ensembles. These findings are consistent with the substitution of the Pt site in PtGe with Co and Cu. The electronic state of Pt was also investigated using X-ray photoelectron spectroscopy (XPS). The Pt $4f_{7/2}$ binding energy of PtGe (72.1 eV) was higher than that of Pt (71.4 eV), depicting that the electron density of Pt was decreased by alloying with Ge and is consistent with the observation in literature (*24*, *25*). On the contrary, the binding energy shifted lower from PtGe to HEI(0.25) (71.6 eV), which suggests that the electron density of Pt was recovered upon multi-metallization. Similar trends in the electron density were also observed in the XANES (white line intensity; PtGe > HEI(0.25) > Pt, Fig. 1C) and FT-IR studies (frequency of linear CO on Pt; PtGe > HEI, Fig. 1F). Note that electron-enriched Pt is also beneficial for selective PDH because propylene desorption is facilitated (*26*, *27*). We also used an *in-situ* XAFS approach to explore the stability of the HEI phase at high temperatures, finding that the PtGe-type structure of HEI(0.25) was preserved even at 700°C (fig. S8). Thus, we successfully synthesized the PtGe-type HEI, which provides thermally stable single-atom Pt as an ideal active site for high-temperature PDH. We also prepared an SAA (Cu–Pt/Ca–SiO_2, Cu/Pt = 25) and quinary HEA (PtFeCoCuGa/Ca–SiO_2) catalyst as control

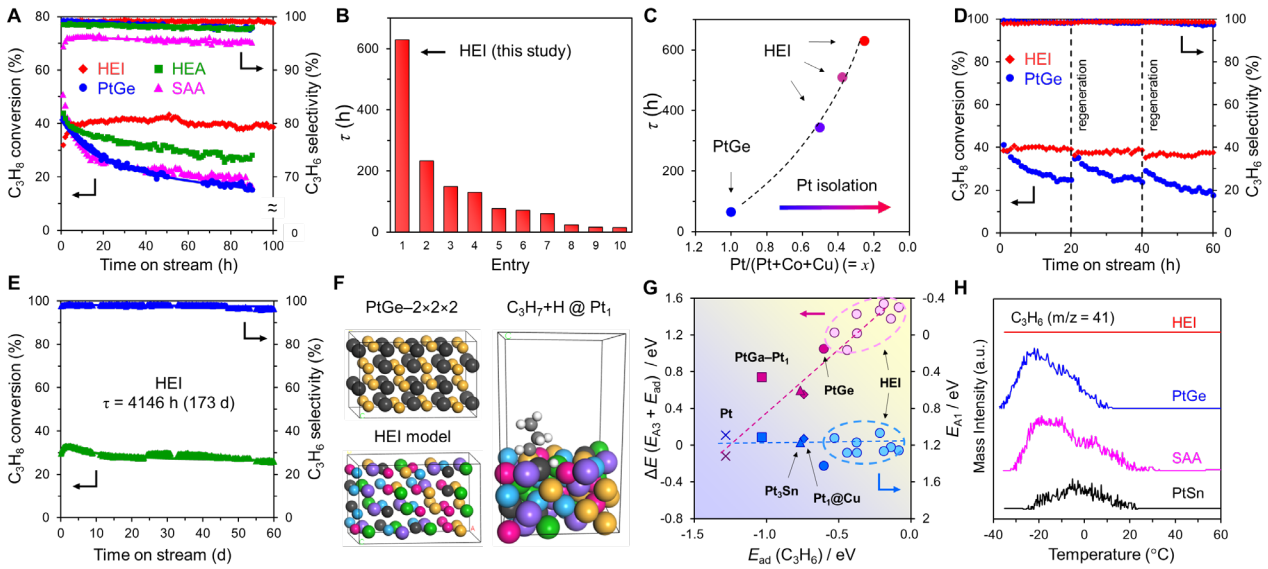

Fig. 2. Catalytic performance of HEI in PDH and DFT calculations. (**A**) Catalytic performances of PtGe, HEI(0.25), SAA, and HEA in PDH at 600°C without co-feeding H_2. (**B**) Mean catalyst life ($\tau = k_d^{-1}$) of reported catalysts and HEI(0.25) in PDH without co-fed H_2 (references are listed in tables S9-S10). (**C**) Relationship between mean catalyst life ($\tau = k_d^{-1}$) and the degree of Pt isolation represented by x as Pt/(Pt+Co+Cu) molar ratio in PtGe and HEI. (**D**) Reusability of PtGe and HEI(0.25) in PDH at 600°C after repeated regeneration processes. (**E**) Long-term stability test of the HEI(0.25) in PDH at 600°C with co-feeding H_2 (catalyst: 150 mg, C_3H_8:H_2:He = 2.5:1.3:3.7 mLmin^{-1}). (**F**) Model structure of HEI (left bottom) derived from PtGe (left top) for DFT calculations. An example of the HEI slab model for PDH: C_3H_7+H at a Pt_1 site (right). (**G**) Relationship between E_{ad} (C_3H_6) and ΔE or E_{A1} for various Pt-based surfaces. (**H**) C_3H_6-TPD for Pt-based catalysts (adsorption temperature: −40°C).

catalysts. The XRD and XAFS analyses confirmed that each catalyst had an fcc structure with high phase purity (figs. S9-12 and Supplementary Text 3). Moreover, Pt atoms in the SAA were sufficiently isolated (table S6). Besides, the corresponding quaternary alloys (PtCoCuGe/Ca–SiO_2 and PtCoCuGa/Ca–SiO_2) were prepared. Interestingly, the Ge-containing quaternary alloy had the PtGe-type intermetallic structure, i.e., (PtCoCu)Ge (figs. S13-14 and Supplementary Text 4), whereas the Ga-containing one showed an fcc solid solution phase (figs. S12, S15-16, and Supplementary Text 4). This is probably due to the large difference in ΔH_f between PtGe (−90.8 kJ mol^{-1}) (*19*) and PtGa (−55.6 kJ mol^{-1}) (*28*). As mentioned for Scheme 1, the significant contribution of the enthalpic term of PtGe seemed to prevail over the entropic effect to form a solid-solution phase upon multi-metallization, while that of PtGa did not. This interpretation is also valid to understand the difference between HEI(0.25) and the quinary HEA.

Then, we tested the catalytic performances of the prepared catalysts in PDH under a considerably harsh condition (600°C, without co-feeding H_2). The SAA catalyst and PtGe were deactivated within 20 h (Fig. 2A) due to the aggregation of nanoparticles (fig. S17) and coke accumulation (fig. S18 and table S7), respectively. The quinary HEA and quaternary catalysts also showed slow deactivation due to coking (Fig. 2A, fig. S19, and table S7). Conversely, HEI(0.25) was not deactivated within 100 h (Fig. 2A) and retained >30% conversion and 99% propylene selectivity up to 260 h (fig. S20), where the mean catalyst life τ (reciprocal deactivation constant k_d^{-1}) was 628 h (table S8). Moreover, HEI(0.25) also exhibited good stability at 620°C (>40% conv. for 120 h, fig. S21). Control experiments were also conducted in PDH using some Pt-based binary alloys (Supplementary Text 5); however, none of them afforded better stability than HEI(0.25) (figs. S22-23 and table S8). To the best of our knowledge, the HEI catalyst exhibited the highest stability in PDH in the absence of H_2 (Fig. 2B, details are listed in tables S9-S10). The particle size distribution did not change before and after the 100-hour catalytic run (figs. S2 and S24), indicating high thermal stability and strong resistance to sintering HEI, according to the HAADF-STEM analysis. We also tested HEI(0.375) and HEI(0.5) in PDH, which resulted in lower selectivity and stability (fig. S25 and table S8). As shown in Fig. 2C, a strong positive correlation was observed between the Pt fraction x and the mean catalyst life τ, indicating that the degree of Pt isolation in HEI determines the selectivity and stability in PDH. Thus, these results demonstrated the validity of our catalyst design concept based on HEIs for high-temperature PDH. A control experiment using the Ca–SiO_2 support was also performed at 600°C, where a small amount of propane was converted to propylene with low selectivity (conv., ~5%; sel., ~70%, fig. S26). This is probably due to a small contribution of noncatalytic thermal cracking (*29*).

We subsequently investigated the reusability of the prepared catalysts through repeated regeneration processes (O_2–H_2 treatments, Fig. 1D). The catalytic activity of PtGe was recovered after the first regeneration procedure, indicating that this treatment could combust the accumulated coke. However, it was not fully recovered despite repeated regeneration, most likely due to irreversible catalyst decomposition. Conversely, HEI(0.25) showed no deactivation after the repeated regeneration procedures, revealing its high durability in repeated regeneration and reuse. Then, the long-term stability of HEI(0.25) was examined in the presence of co-fed H_2 to minimize the coke formation, which is a more common condition for PDH. Notably, HEI(0.25) exhibited outstandingly high stability at 600°C for the first time; little deactivation was observed for at least 2 months (Fig. 2E), where the mean catalyst life (τ = 4146 h) was 1.4 times higher than the highest ever reported (τ = 3067 h) (tables S11-12). Thus, the HEI(0.25) catalyst is the most stable PDH catalyst under different conditions to the best of our knowledge. The coke amount was drastically decreased by co-feeding H_2 (fig. S18) due to the decoking effect of H_2 (coke hydrogenation) (*29*).

Finally, we used DFT computations to ascertain the origin of HEI's exceptional catalytic performance. For PtGe, the (020) plane was considered as the main active surface because it is one of the major facets of PtGe crystal (see fig. S27 and table S13 for the result of Wulff construction) and much more active for C–H scissions than the most stable (211) plane (figs. S28-34 and table S14). The HEI(0.25) structure was modeled based on the PtGe–(2×2×2) supercell, where the Pt and Ge sites were substituted partially and randomly with Co/Cu and Ga/Sn, respectively, such that the Pt faction x was 0.25 (Fig. 2F). Here, we randomly generated twenty structures and chose the most stable one as

an energetically favorable model (table S15). Then, for slab models, two HEI(040) surfaces were considered, each with four distinct isolated Pt atoms and eight Pt–Co/Cu bridge sites for H adsorption (fig. S35). On each Pt–Co/Cu site, the stepwise C–H scissions from C_3H_8 to C_3H_5 were calculated (Fig. 2F right, figs. S36-S59, and table S16). Similar computations were also executed on the (111) surfaces of Pt, Pt_3Sn, and Cu–Pt_1 for comparison (figs. S60-S68 and table S16, results of PtGa were reproduced from the previous study (*30*)). The third C–H scission triggers propylene decomposition, leading to selectivity decrease, coke formation, and consequent catalyst deactivation. Therefore, the propylene selectivity (and catalyst stability) generally depends on the difference in the energy barriers between the third C–H scission and propylene desorption ($\Delta E = E_{A3} - E_d = E_{A3} + E_{ad}$) (*8*, *30*, *31*). The calculated ΔE were in the following order; Pt (−0.11 eV) << Pt_1@Cu (0.55 eV) ≈ Pt_3Sn (0.60 eV) < Pt_1@PtGa (0.74 eV) < PtGe(020) (1.05 eV) < HEI(040) (1.04~1.54 eV) (Fig. 2G and table S16), which is consistent with the experimental trend in propylene selectivity (table S8). Although the ΔE values for HEI varied depending on the site, they were much higher than those on other bimetallic surfaces, indicating exceptional selectivity and stability. Overall, ΔE linearly increased with the E_{ad} (Fig. 2G), indicating that the adsorption strength of propylene on the surface indicates ΔE. Fig. 2G also describes that E_{A1} did not vary depending on the surface, consistent with the structure-insensitivity of PDH. These results suggest that the single-atom Pt on HEI can selectively catalyze propane's first and second C–H scissions, while effectively inhibiting the third one and subsequent side reactions by facile propylene desorption. Notably, no significant difference was observed in the *d*-band shapes and centers between PtGe and HEI(0.25) (fig. S69). Therefore, the weakened propylene adsorption can be attributed to a geometric ensemble effect due to the Pt isolation rather than an electronic effect upon multi-metallization.

Guided by the theoretical study outlined above, we conducted temperature-programmed propylene desorption (C_3H_6-TPD, Fig. 2H) with an adsorption temperature of −35°C (12 °C above the boiling point). PtGe, PtSn, and Cu–Pt SAA exhibited broad desorption peaks between at −40~20°C, where the peak tops appeared in this order. Conversely, no desorption was observed on HEI(0.25), indicating that propylene could not be adsorbed even at −35°C. This trend agrees with that of E_{ad} and demonstrates the remarkably easy desorption of propylene from HEI. We also used CO-TPD, which revealed a similar pattern (fig. S70). As a result, the Pt isolation using HEIs allows for months of selective and continuous propylene production via PDH.

REFERENCES AND NOTES

1. J. J. H. B. Sattler, J. Ruiz-Martinez, E. Santillan-Jimenez, B. M. Weckhuysen, Catalytic dehydrogenation of light alkanes on metals and metal oxides. *Chem. Rev.* **114**, 10613–10653 (2014).
2. Z. P. Hu, D. Yang, Z. Wang, Z. Y. Yuan, State-of-the-art catalysts for direct dehydrogenation of propane to propylene. *Chinese J. Catal.* **40**, 1233–1254 (2019).
3. S. Chen, C. Pei, G. Sun, Z.-J. Zhao, J. Gong, Nanostructured Catalysts toward Efficient Propane Dehydrogenation. *Accounts Mater. Res.* **1**, 30–40 (2020).
4. G. Wang, X. Zhu, C. Li, Recent Progress in Commercial and Novel Catalysts for Catalytic Dehydrogenation of Light Alkanes. *Chem. Rec.* **20**, 604–616 (2020).
5. S. Liu, B. Zhang, G. Liu, Metal-based catalysts for the non-oxidative dehydrogenation of light alkanes to light olefins. *React. Chem. Eng.* (2020).
6. S. Chen, X. Chang, G. Sun, T. Zhang, Y. Xu, Y. Wang, C. Pei, J. Gong, Propane dehydrogenation: catalyst development, new chemistry, and emerging technologies. *Chem. Soc. Rev.* **50**, 3315–3354 (2021).
7. A. H. Motagamwala, R. Almallahi, J. Wortman, V. O. Igenegbai, S. Linic, Stable and selective catalysts for propane dehydrogenation operating at thermodynamic limit. *Science*. **373**, 217–222 (2021).
8. G. Sun, Z. J. Zhao, R. Mu, S. Zha, L. Li, S. Chen, K. Zang, J. Luo, Z. Li, S. C. Purdy, A. J. Kropf, J. T. Miller, L. Zeng, J. Gong, Breaking the scaling relationship via thermally stable Pt/Cu single atom alloys for catalytic dehydrogenation. *Nat. Commun.* **9**, 4454 (2018).
9. J. W. Yeh, S. K. Chen, S. J. Lin, J. Y. Gan, T. S. Chin, T. T. Shun, C. H. Tsau, S. Y. Chang, Nanostructured high-entropy alloys with multiple principal elements: Novel alloy design concepts and outcomes. *Adv. Eng. Mater.* **6**, 299–303 (2004).
10. B. Cantor, I. T. H. Chang, P. Knight, A. J. B. Vincent, Microstructural development in equiatomic multicomponent alloys. *Mater. Sci. Eng. A*. **375**–**377**, 213–218 (2004).
11. E. P. George, W. A. Curtin, C. C. Tasan, High entropy alloys: A focused review of mechanical properties and deformation mechanisms. *Acta Mater.* **188**, 435–474 (2020).
12. Y. Xin, S. Li, Y. Qian, W. Zhu, H. Yuan, P. Jiang, R. Guo, L. Wang, High-Entropy Alloys as a Platform for Catalysis: Progress, Challenges, and Opportunities. *ACS Catal.* **10**, 11280–11306 (2020).
13. P. N. Duchesne, Z. Y. Li, C. P. Deming, V. Fung, X. Zhao, J. Yuan, T. Regier, A. Aldalbahi, Z. Almarhoon, S. Chen, D. en Jiang, N. Zheng, P. Zhang, Golden single-atomic-site platinum electrocatalysts. *Nat. Mater.* **17**, 1033–1039 (2018).
14. G. Firstova, A. Timoshevski, T. Kosorukova, Y. Koval, Y. Matviychuk, P. Verhovlyuk, Electronic and crystal structure of the high entropy TiZrHfCoNiCu intermetallics undergoing martensitic transformation. *MATEC Web Conf.* **33**, 0–3 (2015).
15. N. Zhou, S. Jiang, T. Huang, M. Qin, T. Hu, J. Luo, Single-phase high-entropy intermetallic compounds (HEICs): bridging high-entropy alloys and ceramics. *Sci. Bull.* **64**, 856–864 (2019).
16. K. Yao, L. Liu, J. Ren, Y. Guo, Y. Liu, Y. Cao, R. Feng, F. Wu, J. Qi, J. Luo, P. K. Liaw, W. Chen, High-entropy intermetallic compound with ultra-high strength and thermal stability. *Scr. Mater.* **194**, 113674 (2021).
17. Z. Jia, T. Yang, L. Sun, Y. Zhao, W. Li, J. Luan, F. Lyu, L. C. Zhang, J. J. Kruzic, J. J. Kai, J. C. Huang, J. Lu, C. T. Liu, A Novel Multinary Intermetallic as an Active Electrocatalyst for Hydrogen Evolution. *Adv. Mater.* **32**, 1–9 (2020).
18. T. A. Kosorukova, G. Gerstein, V. V. Odnosum, Y. N. Koval, H. J. Maier, G. S. Firstov, Microstructure formation in cast TiZrHfCoNiCu and CoNiCuAlGaIn high entropy shape memory alloys: A comparison. *Materials (Basel).* **12** (2019).
19. W. G. Jung, O. J. Kleppa, Standard molar enthalpies of formation of Hf_3Ge_2, MeGe (Me = Ir, Pt) and Pt_2Ge. *J. Alloys Compd.* **176**, 301–308 (1991).
20. F. Zaera, *Probing catalytic reactions at surfaces* (2001), vol. 69.
21. K. Ding, A. Gulec, A. M. Johnson, N. M. Schweitzer, G. D. Stucky, L. D. Marks, P. C. Stair, Identification of active sites in CO oxidation and water-gas shift over supported Pt catalysts. *Science*. **350**, 189–192 (2015).
22. X. Zheng, H. Lin, J. Zheng, X. Duan, Y. Yuan, Lanthanum oxide-modified Cu/SiO_2 as a high-performance catalyst for chemoselective hydrogenation of dimethyl oxalate to ethylene glycol. *ACS Catal.* **3**, 2738–2749 (2013).
23. M. J. Dees, T. Shido, Y. Iwasawa, V. Ponec, Infrared studies of CO adsorbed on supported PtCo catalysts. *J. Catal.* **124**, 530–540 (1990).
24. R. Bouwman, P. Biloen, Valence State and Interaction of Platinum and Germanium on y-Al_2O_3 Investigated by X-ray Photoelectron Spectroscopy. *J. Catal.* **48**, 209–216 (1977).
25. S. Rimaz, C. Luwei, S. Kawi, A. Borgna, Promoting effect of Ge on Pt-based catalysts for dehydrogenation of propane to propylene. *Appl. Catal. A Gen.* **588**, 117266 (2019).
26. F. Jiang, L. Zeng, S. Li, G. Liu, S. Wang, J. Gong, Propane Dehydrogenation over Pt/TiO_2-Al_2O_3 Catalysts. *ACS Catal.* **5**, 438–447 (2015).
27. J. Liu, Y. Yue, H. Liu, Z. Da, C. Liu, A. Ma, J. Rong, D. Su, X. Bao, H. Zheng, Origin of the Robust Catalytic Performance of Nanodiamond-Graphene-Supported Pt Nanoparticles Used in the Propane Dehydrogenation Reaction. *ACS Catal.* **7**, 3349–3355 (2017).
28. W. E. Liu, S. E. Mohney, Condensed phase equilibria in transition metal-Ga-Sb systems and predictions for thermally stable contacts to GaSb. *J. Electron. Mater.* **32**, 1090–1099 (2003).
29. Y. Nakaya, F. Xing, H. Ham, K. Shimizu, S. Furukawa, Doubly Decorated Platinum–Gallium Intermetallics as Stable Catalysts for Propane Dehydrogenation. *Angew. Chem. Int. Ed.* **60**, 19715–19719 (2021).
30. Y. Nakaya, J. Hirayama, S. Yamazoe, K. Shimizu, S. Furukawa, Single-atom Pt in intermetallics as an ultrastable and selective catalyst for propane dehydrogenation. *Nat. Commun.* **11**, 2838 (2020).
31. S. Zha, G. Sun, T. Wu, J. Zhao, Z. J. Zhao, J. Gong, Identification of Pt-based catalysts for propane dehydrogenation: Via a probability analysis. *Chem. Sci.* **9**, 3925–3931 (2018).

ACKNOWLEDGEMENTS

Funding: This work was supported by JSPS KAKENHI (Grant Numbers 17H04965, 20H02517, and 21J20594), MEXT project Element Strategy Initiative (JPMXP0112101003), JST PRESTO (JPMJPR19T7), and JST CREST (JPMJCR17J3). The XAFS analysis was performed at the BL01B1 (No. 2020A0611, 2021A1387, and 2021A1571) and BL14B2 (2021A1541) beamlines of Spring-8 at the Japan Synchrotron Radiation Research Institute (JASRI). Synchrotron XRD was carried out at the BL19B2 (2021A2023) beamlines of Spring-8 at the JASRI. We appreciate the technical staffs of the faculty of engineering and Mr. Kah Wei Ting, Hokkaido University for help with HAADF-STEM observation and XPS measurement, respectively. **Author contributions:** S.F. and Y.N. conceived the idea and designed the research and co-wrote the manuscript. Y.N. and E.H. performed catalyst synthesis and PDH reactions. Y.N., E.H, S.F., and H.A. carried out the XAFS measurement. Y.N. conducted the EXAFS curve fitting and most of the other experimental characterizations. S.F. performed the DFT calculations. S.F., Y.N., E.H., H.A., and K.S. discussed the data and commented on the manuscript. **Competing interests:** The authors declare no competing interests. **Data and materials availability:** The data that support the findings of this study are available from the corresponding author upon reasonable request.